Published in final edited form as:

Cell Rep. 2025 April 22; 44(4): 115468. doi:10.1016/j.celrep.2025.115468.

Homeostatic regulation of nucleoporins is a central driver of nuclear pore biogenesis

Stephen Sakuma[1,3], **Marcela Raices**[1], **Ethan Y.S. Zhu**[1,4], **Dana Mamriev**[1], **Charles I. Fisher**[2], **Susanne Heynen-Genel**[1,2], **Maximiliano A. D'Angelo**[1,5,*]

[1]Cancer Metabolism and Microenvironment Program, NCI-designated Cancer Center, Sanford Burnham Prebys Medical Discovery Institute, La Jolla, CA 92037, USA

[2]Conrad Prebys Center for Chemical Genomics, Sanford Burnham Prebys Medical Discovery Institute, La Jolla, CA 92037, USA

[3]Present address: NOMIS Center for Immunobiology and Microbial Pathogenesis, Salk Institute for Biological Studies, La Jolla, CA 92037, USA

[4]Present address: Department of Cell Biology and Pathology, New York University Grossman School of Medicine, New York, NY 10016, USA

[5]Lead contact

SUMMARY

Nuclear pore complexes (NPCs) are channels that control access to the genome. The number of NPCs that cells assemble varies between different cell types and in disease. However, the mechanisms regulating NPC formation in mammalian cells remain unclear. Using a genome-wide small interfering RNA (siRNA) screen, we identify translation-related factors, proteasome components, and the CCR4-NOT complex as top regulators of NPC assembly and numbers. While inhibition of ribosomal function and protein translation reduces NPC formation, blocking protein degradation or CCR4-NOT function increases NPC numbers. We demonstrate that CCR4-NOT inhibition raises global mRNA levels, increasing the pool of nucleoporin mRNAs available for translation. Upregulation of nucleoporin complexes in CCR4-NOT-inhibited cells allows for higher NPC formation, increasing total NPC numbers in normal and cancer cells. Our findings uncover that nucleoporin mRNA stability and protein homeostasis are major determinants of NPC formation and highlight a role for the CCR4-NOT complex in negatively regulating NPC assembly.

*Correspondence: mdangelo@sbpdiscovery.org.

AUTHOR CONTRIBUTIONS

S.S., methodology, investigation, formal analysis, validation, funding acquisition, writing – original draft, and writing – review & editing; M.R., methodology, investigation, formal analysis, validation, and editing; E.Y.S.Z., formal analysis, investigation, and validation; D.M., formal analysis and validation; C.I.F., investigation, formal analysis, and validation; S.H.-G., methodology, formal analysis, and supervision; M.A.D., conceptualization, methodology, supervision, funding acquisition, investigation, validation, project administration, writing - review & editing.

DECLARATION OF INTERESTS

The authors declare that they have no competing interests.

SUPPLEMENTAL INFORMATION

Supplemental information can be found online at https://doi.org/10.1016/j.celrep.2025.115468.

Graphical abstract

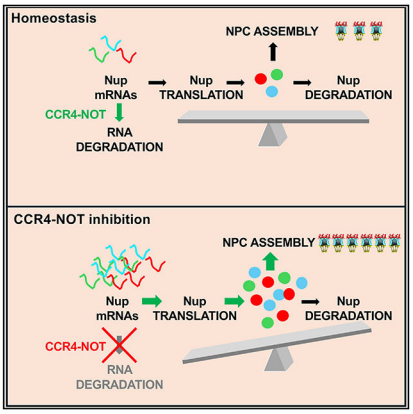

In brief

Sakuma et al. reveal that nucleoporin translation and degradation are main mechanisms regulating nuclear pore complex (NPC) assembly and numbers. They also identify a new role for the CCR4-NOT complex negatively regulating NPC assembly by promoting mRNA degradation and decreasing the levels of available nucleoporins.

INTRODUCTION

Nuclear pore complexes (NPCs) are large protein channels that connect the nucleus with the cytoplasm and mediate the exchange of molecules between these compartments. NPCs also play many transport-independent functions, such as the regulation of chromatin organization, gene expression, cell signaling, and post-translational modifications.[1] The number of NPCs assembled by cells is regulated and can vary significantly across cell types, cellular states, developmental stages, environmental conditions, and even across different species, sometimes by orders of magnitude.[2–7] Changes in NPC numbers have been described during the cell cycle,[4] development,[5] cardiomyocyte maturation,[8] lymphocyte activation,[6,7] and in cancer,[9,10] where large numbers of NPCs are believed to support the increased growth and metabolic demands of transformed cells. Despite the paramount importance of NPCs for cellular homeostasis and survival and their connections to human disease, the cellular mechanisms that drive NPC assembly in mammalian cells remain largely unknown.

NPCs are large protein complexes containing an estimated 1,000 total polypeptides in mammalian cells.[11–13] Remarkably, NPC composition in yeast and mammals is rather simple with these structures being built by the repetition of ~30 different proteins known as nucleoporins.[14,15] Because of the 8-fold rotational symmetry of NPCs, nucleoporins are present in multiples of eight copies,[16] and most of these proteins associate in bio-chemically stable subcomplexes that act as the building blocks for assembly. In mammalian cells, there are two types of NPC assembly processes that take place at different stages of the cell cycle.[17] Post-mitotic NPC assembly occurs at the end of mitosis concomitantly with the reformation of the daughter's nuclear envelope.[18] During this process, NPCs are assembled

by recycling nucleoporins from the mother cell. Interphase NPC assembly takes place from G1 to G2 phases and it doubles the number of nuclear pores to prepare cells for the next division cycle.[19] Although the post-mitotic and interphase NPC assembly processes end in the formation of the same structure, they differ in their assembly mechanisms.[20,21]

Over the past decade, several studies in yeast and mammalian cells have provided insights into how different NPC subcomplexes are assembled and how they come together in a stepwise manner to form NPCs during mitosis and interphase.[12,17,21–23] Multiple studies have also shown that decreased or excessive production of individual nucleoporins can be detrimental to cells and lead to nucleoporin aggregation, nuclear envelope abnormalities, and alterations in NPC formation.[9,12,22,24,25] These data indicate that maintaining the proper levels of NPC components is critical for their formation. However, the mechanisms that mammalian cells employ to ensure the precise quantity of nucleoporins for NPC biogenesis and to define the number of NPCs that will be inserted into the nuclear envelope are mostly unknown.

In this work, we performed a genome-wide small interfering RNA (siRNA) screen to identify regulators of NPC assembly in mammalian cells. We identified protein translation factors (ribosomal proteins, ribosome assembly factors, and eukaryotic initiation factors), proteasome components, and the CCR4-NOT complex (the major regulator of mRNA deadenylation and degradation) as top modulators of NPC formation. We found that depletion of ribosomal/translation-related proteins reduced NPC numbers while downregulation of proteasomal proteins or pharmacological inhibition of protein degradation increased nuclear pore formation. We also discovered that mRNA stabilization by inhibition of the CCR4-NOT complex increases nucleoporin mRNA and protein levels and enhances NPC assembly in normal and cancer cells. Inhibiting protein translation in CCR4-NOT-defective cells blocks the increase in NPC numbers, indicating that modulating nucleoporin steady state mRNA levels directly impacts NPC biogenesis. Our findings show that nucleoporin mRNA and protein degradation restrict NPC assembly and indicate that nucleoporin homeostasis is a major mechanism regulating NPC numbers in mammalian cells.

RESULTS

Whole-genome siRNA screen identifies protein translation and degradation as key modulators of NPC assembly

To identify modulators of NPC assembly, we performed a whole-genome siRNA screen. We developed an imaging-based high-throughput assay based on quantifying changes in NPC staining intensity at the nuclear envelope using the mAb414 antibody, which recognizes four different nucleoporins (NUP62, NUP153, NUP214, and NUP358) from different NPC domains (Figures 1A and 1B). As mentioned above, there are two distinct mechanisms of NPC assembly. Mitotic NPC assembly recycles components from the mother cell, while interphase NPC assembly requires the *de novo* synthesis of new nucleoporins.[21] Because daughter cells will recycle inherited nucleoporins to form NPCs in each cell division, blocking interphase NPC assembly leads to progressive dilution of NPCs as cells divide and distribute their recycled NPCs between their daughter cells.[9] Thus, a minimum of two cell

divisions are required to detect strong changes in NPC numbers when interphase assembly is inhibited. For this reason, human melanoma A375 cells, with a doubling time of <24 h and good staining for NPCs, were reverse transfected with siRNA duplexes and incubated for 48 h before mAb414 antibody staining to allow for gene knockdown and at least two cell divisions. siRNAs against *NUP160*, which we previously showed to strongly inhibit NPC assembly,[9] were used as positive controls (Figure 1B). A longer time point of 72 h was also evaluated but not utilized because high levels of cell death were associated with the assay positive controls, which agrees with the importance of NPC assembly for survival in these cells. Cells were imaged on a confocal high-content screening system and analyzed using a custom-built software analysis script. The main assay parameter was the quantification of NPC signal as determined by the integrated pixel intensity (sum intensity) of mAb414 antibody staining in the nuclear envelope region (Figures 1B and S1A; Table S1). Using A375 cells stably integrated with a doxycycline-inducible short hairpin RNA (shRNA) against *NUP160* we evaluated the NPC assay performance, i.e., sensitivity and robustness, in 384-well plate format by calculating the robust (R) Z' factor of the main assay parameter for vehicle only versus doxycycline-treated cells (Figure S1B). The RZ' factor is less sensitive to outlier wells and is based on the median and median absolute deviation rather than utilizing the mean and SDs of the Z' factor.[26] This resulted in RZ' factors >0.35 for doxycycline concentrations above 15 ng/mL, indicating good assay performance sufficient for high-throughput screening using duplicate wells.

This NPC assay was used for a primary screen of the genome-wide ON TARGET-Plus (OTP) human siRNA library of 18,301 genes with pools of four siRNAs per gene performed in duplicate. Scramble siRNAs and siRNAs against *NUP160* were used as negative and positive controls, respectively, for normalizing the NPC quantification data. A significant difference between the non-targeting scramble siRNAs and the control *NUP160* siRNAs was observed for the screen (Figure S1C), indicating good assay performance. From the screen, we identified genes whose silencing either increased or decreased mAb414 fluorescence sum intensity of the nuclear envelope region. Two limitations of this screening approach should be noted. First, for some genes, a 48-h siRNA treatment may not be sufficient to downregulate protein levels enough to observe an effect on NPC formation. Second, our screen may fail to identify genes with redundant functions in NPC formation, such as Torsins, where the simultaneous knockout of multiple paralog genes is required to observe an effect on NPC assembly.[27]

In our assay, 277 genes showed changes in mAb414 signal at the nuclear envelope with a significance level of $p \leq 0.001$ (Figure 1C). Confirming the validity of the screen, genes coding for NPC components known to be critical for assembly were among the top hits (Figure 1C).[9,28,29] Surprisingly, we found two additional major nodes of regulation of NPC biogenesis, which included ribosomal/translation-related proteins and proteasomal components (Figure 1D; Table S2). While depletion of ribosomal/translation-related proteins reduced NPC numbers, downregulation of proteasomal proteins increased them (Figures 1D and 1E). These data suggest that the balance between protein translation and degradation is a key mechanism regulating NPC numbers. To confirm this, we assessed whether increasing protein levels by pharmacologically inhibiting proteasome activity was sufficient to boost NPC assembly and increase NPC numbers. A375 cells were treated with the proteasome

inhibitors bortezomib, carfilzomib, or MG132, all of which increase protein levels in these cells (Figure S1D), and NPCs were labeled with mAb414 and quantified as described before. We found that inhibition of proteasome activity strongly increased NPC numbers compared to vehicle-treated control cells (Figures 1F and 1G). Our data indicate that the balance between protein translation and degradation is key to NPC formation and positions nucleoporin homeostasis as a major mode of regulating NPC numbers in mammalian cells.

The CCR4-NOT complex negatively regulates NPC assembly

To identify other factors involved in NPC biogenesis, we chose hits outside of the main nodes identified in the primary screen (nucleoporins, ribosomal proteins, or proteasomal proteins). Upon visual inspection of the screen images, we selected 35 promising candidates to be assayed in a secondary screen using the same assay parameters, 23 of which showed the most significant changes in NPC assembly (Figure 2A). Among them, three members of the CCR4-NOT complex, CNOT1, CNOT2, and CNOT3, strongly increased mAb414 staining for NPCs when depleted (Figures 2A–2C), suggesting a role for this complex in negatively regulating NPC formation. To further validate these hits, we repeated the knockdown for the three main components of the complex, CNOT1, CNOT2, and CNOT3, using the four individual siRNAs from the pools used in the screen. Increases in mAb414 staining were observed after knockdown with at least three of the four siRNAs for each gene (Figures S2A–S2C). The CCR4-NOT complex is the primary mRNA deadenylase in mammalian cells and targets mRNAs for deadenylation, thereby regulating their stability and abundance.[30] CNOT1 is the main structural scaffold of the complex and its depletion leads to complex disassembly.[31] CNOT2 and CNOT3 are also structural components but are not essential for the complex's integrity.[31] Since knockdown of CNOT3 had the strongest effect, this gene was selected as a representative member of the CCR4-NOT complex for subsequent studies. CNOT3 depletion with siRNAs was highly efficient and led to strong downregulation of its mRNA and protein levels (Figures S2D–S2F). The increase in NPC levels upon CNOT3 depletion was also confirmed using specific shRNAs (Figure S2G).

CNOT3 depletion strongly increases the number of mature NPCs

The upregulation of mAb414 NPC signal after CNOT3 depletion on single confocal planes was approximately 30% (Figure 2D). These sections represent the signal from only a 1-μm cross-section of the nuclear envelope. To more accurately determine how CNOT3 depletion affects the total number of NPCs per nucleus, we used three-dimensional structured illumination microscopy (3D-SIM), a super-resolution technique that allows imaging and quantification of individual NPCs (Figure 2E).[10,32] Cells were treated with control or CNOT3 siRNAs, fixed, and stained with mAb414 before imaging. Individual NPCs were identified and quantified using the Nikon NIS-Elements software. We found that knockdown of CNOT3 approximately doubled the number of NPCs in the nuclear envelope of A375 cells (average of 2,665 ± 183 and 4,928 ± 458 total NPCs per nucleus of control and CNOT3-depleted cells) (Figure 2E). Our findings indicate that the cross-section quantification of NPC signal accurately reflects the increase and decrease in NPC numbers but significantly underestimates total NPC changes. To determine if the role of CCR4-NOT in modulating NPC numbers is conserved in other cell types, we knocked down CNOT3 in two normal cell lines, human retinal pigment epithelial cells RPE-1 and normal melanocytes

H3A cells. We found that CNOT3 depletion in both cell types increased NPC levels similar to those observed in A375 cells (Figures 2F and 2G). These data demonstrate the CCR4-NOT complex modulates NPC assembly in both cancer and normal cells.

To investigate whether the CCR4-CNOT complex promotes NPC assembly in a particular phase of the cell cycle, we took advantage of the fluorescent ubiquitination-based cell cycle indicator (FUCCI) cell-cycle sensor, which allows the identification of cell-cycle stages by expression of green and red fluorescent reporters (Figure 3A).[33,34] Using this approach, we found a similar fold increase in NPC numbers in G1, S, and G2 (Figure 3B), suggesting that the CNOT3 ablation promotes NPC formation throughout the cell cycle. Analyses of the mAb414 fluorescent intensity of individual NPCs in 3D-SIM images of CNOT3 knockdown cells revealed no differences compared to control cells (Figure 3C). These data indicate that CNOT3 knockdown does not alter the stoichiometry of the mAb414-identified nucleoporins in individual channels and suggest an increase in fully formed NPCs. The formation of NPCs is an ordered process that involves the recruitment of specific nucleoporins from the different subcomplexes at distinct stages of assembly[20,21,35] (Figure S3). Even though the exact sequence and kinetics of recruitment of different nucleoporins and subcomplexes vary between the mitotic and interphase NPC assembly processes, they both end with the addition of cytoplasmic filament protein NUP358[21] (Figure S3). To analyze the composition of NPCs in CNOT3-depleted cells and determine whether they represent mature pores, we examined the levels of individual nucleoporins from distinct subcomplexes by confocal imaging. We found that CNOT3 knockdown increased the nuclear envelope levels of nucleoporins from all substructures of the NPC, including the core scaffold subcomplexes of the outer and inner rings, the central channel, the cytoplasmic filaments, and the nuclear basket (Figures 3D and 3E). The increase in nucleoporins from all NPC domains, including NUP358, the last nucleoporin added during the assembly process, indicates that the NPCs of CNOT3-depleted cells represent fully assembled structures.

CNOT3 knockdown drives NPC assembly by increasing mRNA levels and protein translation

CCR4-NOT is a major deadenylase complex that mediates the shortening of poly(A) tails on eukaryotic mRNA, a key step in mRNA degradation.[30] This complex is capable of regulating both global and transcript-specific mRNA levels.[36–39] A previous study showed that knockdown of CNOT3 selectively increases the stability of distinct mRNAs, which include several nucleoporins such as NUP133, NUP54, NUP37, NUP43, NUP98, CG1, RAE1, NUP50, NUP35, and NUP58.[37] By immunofluorescence quantification, we found that nucleoporins from all major subcomplexes of the NPC are increased at the single-cell level after CNOT3 knockdown (Figure 3E). To determine whether this increase is specific to nucleoporins or due to a more general upregulation of protein translation, we performed a whole-proteome analysis of control cells and cells depleted of CNOT1, CNOT2, or CNOT3 by mass spectrometry (Figure 4A; Figure S4A). In these studies, knockdown of the CCR4-NOT complex members resulted in no changes in nucleoporin protein levels relative to the whole-cell proteome (Figures 4A and 4B). Considering that we found higher levels of nucleoporins in CNOT3-knockdown cells compared to control cells, these findings suggest a more global increase in cellular protein levels. To confirm this, protein extracts from

equal numbers of control and CNOT3-knockdown cells were prepared, and total protein was quantified. We found that CNOT3 depletion strongly increased the amount of total protein per cell (Figure 4C). To further validate this, an equal number of cells were lysed and loaded onto denaturing acrylamide gels. Proteins were separated, stained with Coomassie blue, and the intensity of individual protein bands was quantified. All protein bands detected showed increased levels in the extracts of CNOT3-knockdown cells, consistent with a global increase in protein levels (Figure 4D). The elevated levels of nucleoporin proteins per cell were confirmed by western blot (Figure S4B). We also observed increased levels of LAMIN B, TOM70 (a mitochondrial marker), and S6 (a ribosomal protein) in CNOT3-depleted cells (Figure S4C), suggesting increased levels of these multiprotein complexes. This is further supported by our proteomic analyses showing that components of these structures are upregulated similarly to nucleoporins and is consistent with a broader increase in protein levels (Figure S4D). The higher protein levels in CNOT3-depleted cells were also associated with a similar increase in cell volume (Figure S4E). Additionally, the nuclear surface of these cells showed a smaller ~1.5-fold change (Figure S4E) compared to the 2-fold increase in NPC numbers (Figure 2E), which explains the higher NPC density observed in these cells. The higher density in NPCs was not associated with pore clustering or structural alterations of the nuclear lamina/nuclear envelope (Figure S4F).

Considering the established role of the CCR4-NOT complex in mRNA deadenylation and degradation, we investigated whether the increase in protein levels in CNOT3-knockdown cells resulted from poly(A) mRNA stabilization. To test this, we performed RNA fluorescence *in situ* hybridization (RNA-FISH) using a poly(A) probe and found that CNOT3 depletion strongly increased total mRNA levels (Figures 5A and 5B). To determine whether the upregulation of nucleoporin mRNA levels is due to RNA stabilization, we compared the nucleoporin expression levels after inhibiting transcription with the RNA polymerase II inhibitor α-Amanitin. For this, control and CNOT3-depleted cells were treated with α-Amanitin for 12 h and RNA levels were analyzed by qPCR. At time zero, CNOT3-depleted cells showed increased nucleoporin mRNA levels as well as increased mRNA levels for other genes, including the housekeeping gene HPRT1 and the SRFS3 splicing factor (Figure S5A). Contrarily, GAPDH mRNA was not increased in CNOT3-depleted cells (Figure S5A). These findings confirm that the upregulation of nucleoporin mRNAs is not selective and indicate that, even though CCR4-NOT inhibition results in a broad increase in mRNA levels, not all genes exhibit upregulation. Consistent with mRNA degradation, we found that, upon transcription inhibition, nucleoporin mRNA levels were decreased in both control and CNOT3-depleted cells. However, the fold-change decrease in control cells was significantly higher than in CNOT3-depleted cells, confirming the stabilization of nucleoporin mRNAs in CCR4-CNOT-inhibited cells (Figure 5C). This is consistent with the previous report showing the stabilization of nucleoporin mRNAs by CNOT3 inactivation.[37] mRNA stabilization was also observed for SRSF3, HPRT1, and even GAPDH (Figure S5B). Our findings suggest that inhibition of the CCR4-NOT complex stabilizes nucleoporin mRNAs and promotes NPC assembly upstream of protein translation. If this is the case, reducing protein synthesis in CNOT3-depleted cells should restore NPC numbers to normal. To test this hypothesis, we blocked translation in control and CNOT3-depleted cells with puromycin.[40] We found that puromycin-mediated inhibition

of protein translation effectively blocked the CNOT3 knockdown-induced upregulation of NPC numbers (Figures 5D and 5E). Altogether, these findings indicate the CCR4-NOT complex limits NPC formation by decreasing the pool of nucleoporin mRNAs available for translation.

Higher numbers of NPCs do not increase the nucleocytoplasmic transport rates of CNOT3-depleted cells

Many cancer cells show increased numbers of NPCs and higher nucleocytoplasmic transport.[41–46] Previous studies demonstrated that reducing the number of NPCs results in decreased nucleocytoplasmic transport,[9] but whether increasing NPC numbers is sufficient to drive higher levels of nucleocytoplasmic molecule exchange has not been determined. Taking advantage of the increased NPC numbers resulting from CCR4-NOT complex inactivation, we tested whether CNOT3-depleted cells have higher rates of nuclear import. For this, we generated a stable A375 cell line expressing NLS-2xGFP-NES, a nuclear transport reporter above the size of the NPC permeability barrier. This reporter is actively transported between the nucleus and the cytoplasm and can be used to measure nuclear import rates by fluorescence recovery after photo bleaching (FRAP) assays.[9,47] Using this approach, we found that CNOT3 depletion did not increase the nuclear import of NLS-2xGFP-NES even though the number of NPCs was strongly upregulated (Figure 5F). We also found no differences in nuclear-to-cytoplasmic ratio of the reporter, suggesting no changes in global nuclear export (Figure S5C). Because the A375 cancer cells could have an excess of NPCs, we also tested whether inhibiting CNOT3 increased nuclear transport in normal cells. Similar to A375 cells, we observed no differences in nuclear transport between control and CNOT3-depleted conditions in normal RPE1 and H3A cells (Figure S5D).

DISCUSSION

The NPC channels function as the sole gateway into the nucleus and are essential cellular structures. Besides controlling nucleocytoplasmic molecule exchange, these structures play multiple transport-independent functions that contribute to cellular homeostasis, such as gene expression regulation, mRNA surveillance, and DNA damage repair.[1,48,49] Despite the significant body of research into the molecular composition, order of nucleoporin assembly, and structure of the NPC,[12,21,50] little is still known about the pathways that regulate NPC biogenesis. Here, we performed a whole-genome exploration of regulators of NPC assembly in mammalian cells and identified that the balance between nucleoporin mRNA stability/translation and protein degradation is critical to defining NPC numbers. Our genome-wide screen also uncovered a role for the CCR4-NOT complex in limiting NPC formation in both normal and cancer cells by reducing the levels of nucleoporin mRNAs available for translation.

Our findings indicate that enhancing nucleoporin translation by stabilizing nucleoporin mRNAs through CCR4-NOT inhibition leads to elevated NPC numbers. Additionally, we observed that inhibiting proteasome-mediated protein degradation also boosts NPC numbers. Our data indicate that the degradation of both nucleoporin mRNAs and proteins limits NPC formation, placing nucleoporin proteostasis as a key regulatory mechanism controlling NPC

formation and numbers. NPCs are highly complex structures built by multiple copies of ~30 distinct nucleoporins, most of which are part of stable subcomplexes.[13–15,50,51] The current model in mammals and yeast is that nucleoporin complexes and individual nucleoporins self-assemble to form NPCs.[12,21] Maintaining the proper proportion of nucleoporins and NPC subcomplexes is critical for the formation of these channels since an imbalance of individual NPC components can lead to nucleoporin aggregation, disruption of NPC formation, and cellular alterations that can be detrimental to cells.[9,12,22,24] Emerging evidence shows that cells use two main mechanisms to achieve the proper stoichiometry of multiprotein complex components: proportional protein synthesis and protein buffering by degradation of non-stoichiometric components.[52] Ribosomes are an example of the second mechanism, where complex members are not synthesized proportionally, and non-stoichiometric/orphan components are continually degraded to maintain the proper complex stoichiometry for assembly.[52–54] In this case, blocking the degradation of ribosome components leads to the aggregation of orphan subunits. For NPCs, inhibition of protein degradation results in an increase in NPC numbers, indicating that all critical nucleoporins are synthesized in excess and subsequently degraded. This suggests that the stoichiometry of NPC components is maintained by proportional synthesis. The overproduction of nucleoporins might ensure that their levels are not rate limiting for NPC assembly. It might also represent a mechanism that allows cells to modulate NPC levels by fine-tuning protein degradation. Our findings that proteasome inhibition with bortezomib, which only shows a modest upregulation of total protein levels in our conditions, strongly increases NPC quantity indicate that small changes in protein degradation could be used to modulate NPC numbers. Excess production of nucleoporins might also provide a buffer for other regulatory mechanisms to modulate NPC numbers. For example, the nucleoporin Tpr was previously found to also negatively control NPC formation through ERK-mediated phosphorylation of other NPC components.[10] By producing an excess of nucleoporins ready to be assembled into NPCs, cells could rapidly modify NPC numbers by modulating Tpr/ERK or other regulatory factors without the need to increase the synthesis of new components.

Our screen identified the CCR4-NOT complex as a negative regulator of NPC formation. The main function of the CCR4-NOT complex is to deadenylate mRNAs, decreasing their stability and their availability for translation.[30] This complex can switch between targeted transcript specific and a bulk mRNA degradation depending on the association with different co-factors.[36–39] Our findings indicate that depletion of CNOT1, CNOT2, and CNOT3 in A375 cells result in a global increase in protein levels, including nucleoporins. However, CNOT3 downregulation was also found to selectively regulate the stability of several nucleoporins.[37] This suggests that, in certain cell types or under specific conditions, the CCR4-NOT complex might specifically modulate NPC formation independently of the proteome. Interestingly, members of the yeast and human CCR4-NOT complexes were found to interact with NPC components in an RNA-independent manner, and overexpression of the yeast NOT4 subunit was found to be detrimental to several NPC mutants and to exacerbate their nuclear transport defects.[55,56] These findings are consistent with a CCR4-NOT complex role in regulating NPC formation and raise the exciting possibility that the interaction with nucleoporins might represent a mechanism that allows CCR4-NOT to surveil NPC numbers and adapt its function accordingly. Although positive regulatory

feedback loops for NPC formation have not yet been described in mammalian cells, a recent study in yeast demonstrated the existence of an NPC integrity-sensing mechanism that promotes the translation of nucleoporins in response to NPC alterations.[23] In this positive feedback loop, the loss of small ubiquitin-like modifier (SUMO) protease ULP1 from dysfunctional NPCs leads to the release of nucleoporin mRNAs from the repressing RNA-binding protein HEK1 and increases the synthesis of NPC components.[23] This increase in nucleoporin translation is likely used to promote the formation of new structures to compensate the NPC functional deficiency. A mechanism of promoting NPC biogenesis by upregulating nucleoporin translation is consistent with our findings that mRNA stabilization increases NPC formation in mammals.

Our studies focused on mammalian NPC assembly, but multiple studies show that the mechanisms that regulate this process are conserved in yeast.[50,57,58] *Saccharomyces cerevisiae* has widely been used to investigate NPC biogenesis. This organism divides through close mitosis, and, thus, NPCs only form through the interphase assembly mechanism. Consistent with our findings that post-transcriptional regulation of nucleoporin levels is key to NPC assembly, recent studies support the model that nucleoporin levels in *S. cerevisiae* are mostly controlled at the translation and degradation stage.[12,22,23] Moreover, in this organism, localized translation at NPCs and co-translational assembly of nucleoporin subcomplexes was proposed to contribute to nuclear pore biogenesis by helping to maintain the proper stoichiometry of complex members and preventing the accumulation and aggregation of orphan nucleoporin proteins.[22]

Our findings that increasing NPC numbers by downregulation of CNOT3 is not sufficient to augment nucleocytoplasmic transport suggest that cancer and normal cells have more NPCs than required to ensure efficient nuclear transport rates. This would be consistent with our previous studies showing that nuclear transport alterations are only observed when NPC numbers are reduced by 50%–75% or more.[9] It is also possible that the additional NPCs formed in CNOT3-depleted cells are partially assembled structures that are not active in nucleocytoplasmic transport. Our findings that NPCs in CNOT3 knockdown cells have components of all major subcomplexes that are assembled at different times of the assembly process including NUP358, the final nucleoporin added during NPC formation, argue against this possibility, and suggest that these structures are indeed mature NPCs. Although our findings cannot discard the possibility that increasing NPC numbers could enhance the nuclear import or export of specific molecules, such as oncogenes or tumor suppressors, they raise the possibility that the advantage more NPCs provide to cancer cells might rely on the transport-independent functions of this structures. Additional experiments will be required to establish the physiological benefits that elevated NPC numbers provide to cancer cells and how they contribute to tumorigenesis.

Limitations of the study

A limitation of our study is that our screening approach does not allow us to identify genes that might exhibit functional redundancy in NPC formation. For example, Torsin A has been shown to be required for NPC assembly, but its functional redundancy necessitates the downregulation of multiple isoforms to observe a phenotype.[27] This redundancy could

lead to the underestimation of certain regulators in our analysis. Furthermore, our screen was conducted 48 h post treatment, a time frame that might not capture the effects of stable or slow-acting factors involved in NPC formation. These factors may require longer siRNA incubation times to exert their influence, potentially resulting in their exclusion from our findings. Consequently, while our genome-wide screen is comprehensive, it may have missed some regulators of NPC biogenesis.

In addition to these methodological considerations, there are inherent limitations in our CNOT3 inhibition-based model for studying the physiological consequences of changes in NPC numbers. While we can directly infer the impact of increased NPC numbers on nucleocytoplasmic transport due to their direct connection, broader functional insights remain elusive. Because inhibiting CCR4-NOT leads to broad changes in protein levels, isolating the effects directly attributable to altered NPC numbers is challenging. This complicates the investigation of other NPC functions, such as their roles in gene expression regulation, chromatin organization, or the DNA damage that could be the result of NPC-independent mechanisms triggered by CCR4-NOT inhibition. To study how NPC numbers affect these functions, identifying a method to selectively modulate NPC numbers without inducing global changes in protein expression is essential.

STAR★METHODS

METHOD DETAILS

Cell culture: A375 cells were obtained from ATCC. Puromycin sensitive RPE1 and Hermes 3A (H3A) cells were kindly provided by Dr. A. Holland (John Hopkins University) and Ze'ev Ronai (Sanford Burnham Prebys Medical Discovery Institute) respectively. Cell lines were authenticated by the Sanford Burnham Prebys Genomics Core Facility using the GenePrint10 (Promega) Short Tandem Repeat (STR) DNA genotyping. Cells were routinely tested for Mycoplasma contamination using the MycoAlert Mycoplasma Detection Kit (Lonza, LT07–118). Human A375 and RPE1 cells' sex were female and human H3A cells were male. No influence of sex was detected. All cells were cultured in a humidified 37°C incubator with 5% CO2 in media supplemented with 10% heat-inactivated fetal bovine serum and 100 unit/mL penicillin-streptomycin. A375 cells were cultured in DMEM medium (Mediatech), H3A cells were cultured in RPMI-1640 medium (GE Healthcare Bio Science, Hyclone) and RPE1 cells were cultured in DMEM/F12 medium (Gibco). For siRNA transfection, cells were treated with Lipofectamine RNAiMAX Transfection Reagent (Life Technologies) according to manufacturer's protocol with a final concentration of 40 nM siRNA and grown for 2 days before immunofluorescent staining. For inhibitor treatments, cells were treated with 200 ng/mL puromycin, 1 nM bortezomib, 175 nM carfilzomib, 2.5 mM thymidine, or 1 μM MG132 for 18 h.

Whole-genome siRNA screen: For the whole genome siRNA screen, A375 cells were reverse transfected with 10 nM siRNA pools (Horizon Discovery SMARTpool siRNA library) for individual nucleoporins in 384-well plates by Sanford Burnham Prebys Functional Genomics Core. Cells were fixed 48 h later with 4% paraformaldehyde (PFA) and stained with the mAb414 antibody and Hoechst 33342 as described above. Imaging was

performed at Sanford Burnham Prebys Conrad Prebys Center for Chemical Genomics on an Opera Phenix Screener (PerkinElmer) confocal high content screening system using a 40× 1.1 NA water immersion objective. Acquired images were analyzed using Harmony HCS software (PerkinElmer) as detailed in Table S1 and Figure S1A. The main assay parameter used for selection of active siRNAs was the sum intensity of the nuclear envelope region for the Alexa Fluor 488 immunofluorescently labeled mAb414 antibody. The mAb414 sum intensity of the nuclear envelope was calculated at the single cell level, log transformed and the median of all cells per well was calculated and used as the well-level readout. All siRNA screen plates contained 30 non-specific (NS) siRNA controls wells as well as 7 siNUP160 inhibition control wells. The data was normalized to the control wells and corrected for systemic plate effects using Genedata Screener software. Primary screen hits with a *p*p-value less than 0.001 were analyzed for predicted protein interaction network using the STRING database (version 12) online at https://string-db.org/.

Viral transduction: Virus was prepared by the Sanford Burnham Prebys Viral Vectors Core. Cells were transduced with pTripz tetracycline-inducible shRNA lentivirus (Control RHS4743, NUP160 clone V2THS_101965, CNOT3 clone V2THS_87050 from Dharmacon) or the nuclear transport reporter NLS-2xGFP-NES pLV lentivirus (VB201028–1237ewv from VectorBuilder) followed 2 days later by selection. Selection was performed with 10 μg/mL Blasticidin (Gibco) for the VectorBuilder construct or 1.25 μg/mL Puromycin (Gibco) for Dharamacon constructs. shRNA expression was induced with 0.5 μg/mL doxycycline (Clontech) for 3 days.

Immunofluorescence microscopy: Cells were seeded and grown on polymer coverslip 8-well μSlide dishes (IBIDI) for confocal microscopy and on round cover glass in 24 well plates for 3D Structured Illumination Microscopy (3D-SIM). Cells were fixed in 2% PFA (methanol-free) in PBS for 5 min followed by permeabilization and blocking using IF buffer (1x PBS, 10 mg/mL BSA, 0.02% SDS, 0.1% Triton X-100) for 1 h at room temperature (RT). Cells were then incubated with primary antibody diluted in IF buffer for 1 h at RT or overnight at 4°C and washed with IF buffer. Cells were then incubated with secondary antibody diluted in IF buffer for 1 h at RT and washed with IF buffer. Cells were then incubated with 1 μg/mL Hoechst 33342 in PBS for 5 min and washed with PBS before imaging. Imaging was performed with a Leica SP8 confocal microscope with a 40x oil immersion objective or Nikon N-SIM with 100x oil immersion objective for 3D-SIM in the Sanford Burnham Prebys Cell Imaging Core.

α-amanitin treatment, RNA extraction, and Real-time quantitative PCR - qPCR: For mRNA stability experiments, A375 cells were transfected with control or CNOT3 siRNAs for 72 h before treatment for 12 h with 10 μg/mL of α-amanitin for 12 h. RNA extraction was performed with a PureLink RNA Mini kit (Thermo Fisher Scientific), and 1 μg of RNA was used to synthesize cDNA with a QuantiTect Reverse Transcription Kit (Qiagen). qPCR was carried out with TaqMan Fast Advanced Master Mix (Applied Biosystems). qPCR data were collected on a CFX384 Real-Time PCR Detection System (Bio-Rad) and analyzed using the Bio-Rad CFX Maestro Software version 2.3.

Nuclear transport: For nuclear transport measurements, 10,000 cells of A375, H3A, or RPE1 stably expressing the transport reporter NLS-2xGFP-NES were plated on polymer coverslip 8-well µSlide dishes (IBIDI) and transfected with siRNAs as described above. 48 h after siRNA transfection cells were equilibrated for 1 h in a humidified 37°C with 5% CO2 stage top incubator (H301, Okolab) controlled by the Oko-Touch (Okolab). Cells were then imaged on a Leica DMi8 microscope at 40x magnification. For FRAP, the reporter nuclear signal was photobleached with 50% power 488 nm laser for 3 s, and transport of fluorescent signal was recorded for 2 min using the LAS X software. A total of 18 cells were imaged per condition. Nuclear import data were calculated by dividing the nuclear and cytoplasmic background-subtracted signals and then normalized to the pre-bleach ratio. For nuclear/cytoplasmic ratio of NLS-2xGFP-NES, cells were fixed, permeabilized, and stained for Hoechst 33342 as described above. Cells were then imaged at 40x magnification and the mean intensity in the nucleus divided by the mean intensity in the cytoplasm was quantified.

Western blotting: For protein extracts, cells were washed with ice-cold PBS containing Protease and Phosphatase inhibitors (Pierce Halt Protease and Phosphatase Inhibitor Cocktail, ThermoFisher Scientific) and harvested with RIPA buffer containing Protease and Phosphatase inhibitors. Homogenates were incubated on ice for 30 min and passed 5–10 times though a 29 G syringe to shear DNA. Protein concentration was determined using the Pierce BCA reagent (ThermoFisher Scientific) according to manufacturer directions in triplicate. LDS Sample Buffer premixed with NUPAGE Sample Reducing Agent (Life Technologies) was added, and samples were incubated for 10 min at 70°C. For western blot analysis, 20 or 40 µg of protein were resolved by SDS-PAGE on NUPAGE Novex 3–8% tris-acetate protein gels or Bolt 4–12% Bis-Tris Plus protein gels (Invitrogen) and blotted to nitrocellulose membranes using an iBlot2 Dry Blotting System. Membranes were stained with Ponceau, washed with TBS, and blocked for 1 h at RT with TBS-0.1% Tween 20 (TBS-T) containing 5% nonfat milk, and incubated with primary antibodies overnight at 4°C. After three washes with TBS-T, the secondary antibody was added and incubated for 1 h at RT. Membranes were then washed and developed using the Pierce ECL Western Blotting Substrate (ThermoFisher Scientific).

Protein quantification: One and half million cells were pelleted and washed with ice-cold PBS. Cells were then lysed with 120 µL 2X SDS buffer (240 mM Tris-HCl at pH 6.8, 4% SDS, 16% glycerol + protease inhibitors) preheated to 95°C. Homogenates were passed 5–10 times though a 29 G syringe to shear DNA. Lysates' protein quantification was performed as described above. For Coomassie gel staining, SDS-PAGE was performed as described above using 50,000 cells per well. Gels were stained in Coomassie R250 for 1 h and then destained using 10% acetic acid, 50% methanol, and 40% water overnight. Gels were imaged using the Bio-Rad ChemiDoc Touch.

RNA fluorescence In Situ Hybridization: RNA Fluorescence In Situ Hybridization (RNA-FISH) was performed with Stellaris Poly(A) probes and buffers following the manufacturer's protocol. Briefly, cells were fixed in PBS with 4% PFA for 10 min, washed twice with PBS. After fixation, cells were permeabilized in 70% ethanol for 1 h at 4°C. Cells were subsequently incubated in Buffer A (2xSSC, 10% formamide) at RT for 5 min

and then, hybridized in a humidified chamber with 125 nM probe in hybridization buffer (2xSSC, 10% formamide, 10% dextran sulfate) at 37°C for 16 h. Cells were then washed with Buffer A for 30 min at 37°C twice followed by a 5-min incubation with 6 ng/mL Hoechst in Buffer A. Cells were washed with PBS and imaged.

Proteomics: For proteomics experiments, 0.5 million A375 cells were transfected with siRNA 48 h before collection. Cells were collected by rinsing with PBS and treating with trypsin for 5 min at 37°C. Cells were pelleted by centrifugation and supernatants were removed before liquid nitrogen snap freezing of the pellets. Protein extracts were made by resuspending pellets in 8 M Urea, 50 mM ammonium bicarbonate, benzonase buffer. Proteins were digested with trypsin and column purified. Peptides were then eluted in 2% ACN and 0.1% Formic Acid. To label peptides, tandem mass tag 10plex kits (Thermo Fisher Scientific) were used following the manufacturer's protocol. LC–MS/MS analysis was performed on a Thermo Orbitrap Fusion Lumos Tribrid. Proteomics experiments were carried out in collaboration with the Sanford Burnham Prebys Proteomics core and data analysis was completed by the Sanford Burnham Prebys Bioinformatics core. Proteomics data normalization and group comparisons were performed using MSstatsTMT R package.[60] Data was converted from SpectroMine to MSstatsTMT format using SpectroMinetoMSstatsTMTFormat. Peptide level quantifications were summarized to protein level and data normalized using proteinSummarization with the following options: method = "msstats", global_norm = TRUE, reference_norm = TRUE, remove_norm_channel = TRUE, and remove_empty_channel = TRUE. Pairwise group comparisons were performed using groupComparisonTMT and parameter moderated = TRUE.

Flow cytometry: Analytical cytometry was performed in the Sanford Burnham Prebys Flow Cytometry Core, using the BD LSR Fortessa (BD Biosciences). One million cells were fixed with 70% cold ethanol in PBS for 1 h at −20°C and stained with 2.5 μg/mL Hoechst (Invitrogen) in PBS with 2% FBS before analysis by flow cytometry.

Data collection and analysis: Microsoft Excel was used to record and calculate data. GraphPad Prism 8 software v8.2 (GraphPad Software, Inc.) was used to prepare graphs and to perform statistical analyses. Microscopy data were collected with a DMi8 Leica SP8 confocal microscope and analyzed using the Leica Application Suite X software v3.1.5.16308 (Leica Microsystems) or NIH ImageJ v2.0.0-rc54/1.51h.[59] To analyze confocal fluorescence images, an ImageJ (Fiji) macro was used to identify the nuclear periphery and quantify the intensity of immunofluorescence in the nucleus, at the nuclear envelope, and in the cytoplasm of single cells and values were expressed relative to the mean of the control (Data S1). To analyze 3D-SIM images, NIS-Elements version 5.42.04 Build 1814 was used. For NPC counting, the 3D spot detection module was used with a 0.2 μm diameter spot setting. qPCR data were collected in a CFX384 Real-Time PCR Detection System (Bio-Rad) and analyzed with CFX Maestro Software (V2.3). Flow cytometry data were collected using the BD FACSDIVA Software (BD Biosciences) and analyzed using FlowJo software v10.9.0 (BD Biosciences), and cell cycle distribution was calculated with the Dean-Jett-Fox model.

Data and materials availability: All data supporting the findings of this study are available within the paper and its Supplementary Information. The proteomics data-sets generated during the current study are available at ProteomeXchange biorepository under accession number PXD052767.

QUANTIFICATION AND STATISTICAL ANALYSIS

Data are presented as the mean ± standard deviation (SD). The two-tailed unpaired Student's t-test was used to evaluate differences between two groups. Ordinary one-way analysis of variance (ANOVA) was used for comparing multiple groups to a single control. two-way ANOVA with Sidak multiple comparisons test was used for comparing multiple groups to different controls. Results were considered statistically significant when differences were $p \leq 0.05$ (****$p \leq 0.0001$, ***$p \leq 0.001$, **$p \leq 0.01$, *$p \leq 0.05$; ns indicates not significant). The numbers of independent experiments are shown in the respective figure legends. We conducted all statistical analyses using GraphPad Prism 8 (GraphPad Software, San Diego, CA, USA).

Supplementary Material

Refer to Web version on PubMed Central for supplementary material.

ACKNOWLEDGMENTS

We thank Dr. P. Aza-Blanc for assistance with the siRNA screen. We thank Dr. R. Murad and S. Maurya for assisting with the proteomics studies and data analyses. We also thank Drs. A. Holland and Z. Ronai for providing cell lines used in this work and Dr. J. Zhao for providing proteasome inhibitors. This work was supported by the NIH (F99CA274682) and the American Cancer Society (DBG-24-1319723-01-CCB). This work was also supported by the National Institutes of Health the NCI Cancer Center grant P30CA030199, which supports the Flow Cytometry, Genomics, Bioinformatics, Proteomics, and High Content Screening cores. The content is solely the responsibility of the authors and does not necessarily represent the official views of the NIH.

RESOURCE AVAILABILITY

Lead contact

Further information and requests should be directed to and will be fulfilled by the lead contact, Maximiliano D'Angelo (mdangelo@sbpdiscovery.org).

Materials availability

This study did not generate new unique reagents.

Data and code availability

- Proteomics data generated in this study have been deposited at ProteomeXchange: PXD052767 and are publicly available as of the date of publication.
- This paper does not report original code.
- ImageJ macro developed for quantification is included in Data S1.

- Any additional information required to reanalyze the data reported in this paper is available from the lead contact upon request.

REFERENCES

1. Raices M, and D'Angelo MA (2022). Structure, Maintenance, and Regulation of Nuclear Pore Complexes: The Gatekeepers of the Eukaryotic Genome. Cold Spring Harb. Perspect. Biol 14, a040691. 10.1101/cshperspect.a040691. [PubMed: 34312247]
2. Maul GG, and Deaven L (1977). Quantitative determination of nuclear pore complexes in cycling cells with differing DNA content. J. Cell Biol 73, 748–760. 10.1083/jcb.73.3.748. [PubMed: 406262]
3. Garcia-Segura LM, Lafarga M, Berciano MT, Hernandez P, and Andres MA (1989). Distribution of nuclear pores and chromatin organization in neurons and glial cells of the rat cerebellar cortex. J. Comp. Neurol 290, 440–450. 10.1002/cne.902900311. [PubMed: 2592622]
4. Maeshima K, Iino H, Hihara S, and Imamoto N (2011). Nuclear size, nuclear pore number and cell cycle. Nucleus 2, 113–118. 10.4161/nucl.2.2.15446. [PubMed: 21738834]
5. Shen W, Gong B, Xing C, Zhang L, Sun J, Chen Y, Yang C, Yan L, Chen L, Yao L, et al. (2022). Comprehensive maturity of nuclear pore complexes regulates zygotic genome activation. Cell 185, 4954–4970.e20. 10.1016/j.cell.2022.11.011. [PubMed: 36493774]
6. Maul GG, Maul HM, Scogna JE, Lieberman MW, Stein GS, Hsu BY, and Borun TW (1972). Time sequence of nuclear pore formation in phytohemagglutinin-stimulated lymphocytes and in HeLa cells during the cell cycle. J. Cell Biol 55, 433–447. 10.1083/jcb.55.2.433. [PubMed: 5076782]
7. Maul GG, Price JW, and Lieberman MW (1971). Formation and distribution of nuclear pore complexes in interphase. J. Cell Biol 51, 405–418. [PubMed: 5165267]
8. Han L, Mich-Basso JD, Li Y, Ammanamanchi N, Xu J, Bargaje AP, Liu H, Wu L, Jeong JH, Franks J, et al. (2022). Changes in nuclear pore numbers control nuclear import and stress response of mouse hearts. Dev. Cell 57, 2397–2411.e9. 10.1016/j.devcel.2022.09.017. [PubMed: 36283391]
9. Sakuma S, Raices M, Borlido J, Guglielmi V, Zhu EYS, and D'Angelo MA (2021). Inhibition of Nuclear Pore Complex Formation Selectively Induces Cancer Cell Death. Cancer Discov. 11, 176–193. 10.1158/2159-8290.CD-20-0581. [PubMed: 32988961]
10. McCloskey A, Ibarra A, and Hetzer MW (2018). Tpr regulates the total number of nuclear pore complexes per cell nucleus. Genes Dev. 32, 1321–1331. 10.1101/gad.315523.118. [PubMed: 30228202]
11. Dultz E, Wojtynek M, Medalia O, and Onischenko E (2022). The Nuclear Pore Complex: Birth, Life, and Death of a Cellular Behemoth. Cells 11, 1456. 10.3390/cells11091456. [PubMed: 35563762]
12. Penzo A, and Palancade B (2023). Puzzling out nuclear pore complex assembly. FEBS Lett. 597, 2705–2727. 10.1002/1873-3468.14713. [PubMed: 37548888]
13. Rout MP, Aitchison JD, Suprapto A, Hjertaas K, Zhao Y, and Chait BT (2000). The yeast nuclear pore complex: composition, architecture, and transport mechanism. J. Cell Biol 148, 635–651. [PubMed: 10684247]
14. Cronshaw JM, Krutchinsky AN, Zhang W, Chait BT, and Matunis MJ (2002). Proteomic analysis of the mammalian nuclear pore complex. J. Cell Biol 158, 915–927. [PubMed: 12196509]
15. Petrovic S, Mobbs GW, Bley CJ, Nie S, Patke A, and Hoelz A (2022). Structure and Function of the Nuclear Pore Complex. Cold Spring Harb. Perspect. Biol 14, a041264. 10.1101/cshperspect.a041264. [PubMed: 36096637]
16. Ori A, Banterle N, Iskar M, Andrés-Pons A, Escher C, Khanh Bui H, Sparks L, Solis-Mezarino V, Rinner O, Bork P, et al. (2013). Cell type-specific nuclear pores: a case in point for context-dependent stoichiometry of molecular machines. Mol. Syst. Biol 9, 648. 10.1038/msb.2013.4. [PubMed: 23511206]
17. Otsuka S, and Ellenberg J (2018). Mechanisms of nuclear pore complex assembly - two different ways of building one molecular machine. FEBS Lett. 592, 475–488. 10.1002/1873-3468.12905. [PubMed: 29119545]

18. Otsuka S, Steyer AM, Schorb M, Hériché JK, Hossain MJ, Sethi S, Kueblbeck M, Schwab Y, Beck M, and Ellenberg J (2018). Postmitotic nuclear pore assembly proceeds by radial dilation of small membrane openings. Nat. Struct. Mol. Biol 25, 21–28. 10.1038/s41594-017-0001-9. [PubMed: 29323269]
19. Otsuka S, Bui KH, Schorb M, Hossain MJ, Politi AZ, Koch B, Eltsov M, Beck M, and Ellenberg J (2016). Nuclear pore assembly proceeds by an inside-out extrusion of the nuclear envelope. Elife 5, e19071. 10.7554/eLife.19071. [PubMed: 27630123]
20. Dultz E, and Ellenberg J (2010). Live imaging of single nuclear pores reveals unique assembly kinetics and mechanism in interphase. J. Cell Biol 191, 15–22. 10.1083/jcb.201007076. [PubMed: 20876277]
21. Otsuka S, Tempkin JOB, Zhang W, Politi AZ, Rybina A, Hossain MJ, Kueblbeck M, Callegari A, Koch B, Morero NR, et al. (2023). A quantitative map of nuclear pore assembly reveals two distinct mechanisms. Nature 613, 575–581. 10.1038/s41586-022-05528-w. [PubMed: 36599981]
22. Lautier O, Penzo A, Rouviere JO, Chevreux G, Collet L, Loiodice I, Taddei A, Devaux F, Collart MA, and Palancade B (2021). Co-translational assembly and localized translation of nucleoporins in nuclear pore complex biogenesis. Mol. Cell 81, 2417–2427.e2415. 10.1016/j.molcel.2021.03.030. [PubMed: 33838103]
23. Rouviere JO, Bulfoni M, Tuck A, Cosson B, Devaux F, and Palancade B (2018). A SUMO-dependent feedback loop senses and controls the biogenesis of nuclear pore subunits. Nat. Commun 9, 1665. 10.1038/s41467-018-03673-3. [PubMed: 29695777]
24. Agote-Aran A, Schmucker S, Jerabkova K, Jmel Boyer I, Berto A, Pacini L, Ronchi P, Kleiss C, Guerard L, Schwab Y, et al. (2020). Spatial control of nucleoporin condensation by fragile X-related proteins. EMBO J. 39, e104467. 10.15252/embj.2020104467. [PubMed: 32706158]
25. Meszaros N, Cibulka J, Mendiburo MJ, Romanauska A, Schneider M, and Kohler A (2015). Nuclear pore basket proteins are tethered to the nuclear envelope and can regulate membrane curvature. Dev. Cell 33, 285–298. 10.1016/j.devcel.2015.02.017. [PubMed: 25942622]
26. Zhang JH, Chung TD, and Oldenburg KR (1999). A Simple Statistical Parameter for Use in Evaluation and Validation of High Throughput Screening Assays. J. Biomol. Screen 4, 67–73. 10.1177/108705719900400206. [PubMed: 10838414]
27. Laudermilch E, Tsai PL, Graham M, Turner E, Zhao C, and Schlieker C (2016). Dissecting Torsin/cofactor function at the nuclear envelope: a genetic study. Mol. Biol. Cell 27, 3964–3971. 10.1091/mbc.E16-07-0511. [PubMed: 27798237]
28. Walther TC, Alves A, Pickersgill H, Loïodice I, Hetzer M, Galy V, Hülsmann BB, Köcher T, Wilm M, Allen T, et al. (2003). The conserved Nup107–160 complex is critical for nuclear pore complex assembly. Cell 113, 195–206. [PubMed: 12705868]
29. Grandi P, Dang T, Pané N, Shevchenko A, Mann M, Forbes D, and Hurt E (1997). Nup93, a vertebrate homologue of yeast Nic96p, forms a complex with a novel 205-kDa protein and is required for correct nuclear pore assembly. Mol. Biol. Cell 8, 2017–2038. [PubMed: 9348540]
30. Pavanello L, Hall M, and Winkler GS (2023). Regulation of eukaryotic mRNA deadenylation and degradation by the Ccr4-Not complex. Front. Cell Dev. Biol 11, 1153624. 10.3389/fcell.2023.1153624. [PubMed: 37152278]
31. Shirai YT, Suzuki T, Morita M, Takahashi A, and Yamamoto T (2014). Multifunctional roles of the mammalian CCR4-NOT complex in physiological phenomena. Front. Genet 5, 286. 10.3389/fgene.2014.00286. [PubMed: 25191340]
32. Schermelleh L, Carlton PM, Haase S, Shao L, Winoto L, Kner P, Burke B, Cardoso MC, Agard DA, Gustafsson MGL, et al. (2008). Subdiffraction multicolor imaging of the nuclear periphery with 3D structured illumination microscopy. Science 320, 1332–1336. 10.1126/science.1156947. [PubMed: 18535242]
33. Sakaue-Sawano A, Kurokawa H, Morimura T, Hanyu A, Hama H, Osawa H, Kashiwagi S, Fukami K, Miyata T, Miyoshi H, et al. (2008). Visualizing spatiotemporal dynamics of multicellular cell-cycle progression. Cell 132, 487–498. 10.1016/j.cell.2007.12.033. [PubMed: 18267078]
34. Sakaue-Sawano A, and Miyawaki A (2014). Visualizing spatiotemporal dynamics of multicellular cell-cycle progressions with fucci technology. Cold Spring Harb. Protoc 2014, pdb.prot080408. 10.1101/pdb.prot080408.

35. Otsuka S, Szymborska A, and Ellenberg J (2014). Imaging the assembly, structure, and function of the nuclear pore inside cells. Methods Cell Biol. 122, 219–238. 10.1016/B978-0-12-417160-2.00010-2. [PubMed: 24857732]
36. Collart MA, and Struhl K (1994). NOT1(CDC39), NOT2(CDC36), NOT3, and NOT4 encode a global-negative regulator of transcription that differentially affects TATA-element utilization. Genes Dev. 8, 525–537. 10.1101/gad.8.5.525. [PubMed: 7926748]
37. Suzuki T, Kikuguchi C, Sharma S, Sasaki T, Tokumasu M, Adachi S, Natsume T, Kanegae Y, and Yamamoto T (2015). CNOT3 suppression promotes necroptosis by stabilizing mRNAs for cell death-inducing proteins. Sci. Rep 5, 14779. 10.1038/srep14779. [PubMed: 26437789]
38. Raisch T, and Valkov E (2022). Regulation of the multisubunit CCR4-NOT deadenylase in the initiation of mRNA degradation. Curr. Opin. Struct. Biol 77, 102460. 10.1016/j.sbi.2022.102460. [PubMed: 36116370]
39. Raisch T, Chang CT, Levdansky Y, Muthukumar S, Raunser S, and Valkov E (2019). Reconstitution of recombinant human CCR4-NOT reveals molecular insights into regulated deadenylation. Nat. Commun 10, 3173. 10.1038/s41467-019-11094-z. [PubMed: 31320642]
40. Hobson BD, Kong L, Hartwick EW, Gonzalez RL, and Sims PA (2020). Elongation inhibitors do not prevent the release of puromycylated nascent polypeptide chains from ribosomes. Elife 9, e60048. 10.7554/eLife.60048. [PubMed: 32844746]
41. Pathria G, Wagner C, and Wagner SN (2012). Inhibition of CRM1-mediated nucleocytoplasmic transport: triggering human melanoma cell apoptosis by perturbing multiple cellular pathways. J. Invest. Dermatol 132, 2780–2790. 10.1038/jid.2012.233. [PubMed: 22832492]
42. Kim J, McMillan E, Kim HS, Venkateswaran N, Makkar G, Rodriguez-Canales J, Villalobos P, Neggers JE, Mendiratta S, Wei S, et al. (2016). XPO1-dependent nuclear export is a druggable vulnerability in KRAS-mutant lung cancer. Nature 538, 114–117. 10.1038/nature19771. [PubMed: 27680702]
43. Lewin JM, Lwaleed BA, Cooper AJ, and Birch BR (2007). The direct effect of nuclear pores on nuclear chemotherapeutic concentration in multidrug resistant bladder cancer: the nuclear sparing phenomenon. J. Urol 177, 1526–1530. 10.1016/j.juro.2006.11.048. [PubMed: 17382772]
44. Kuusisto HV, Wagstaff KM, Alvisi G, Roth DM, and Jans DA (2012). Global enhancement of nuclear localization-dependent nuclear transport in transformed cells. FASEB J. 26, 1181–1193. 10.1096/fj.11-191585. [PubMed: 22155563]
45. Rodriguez-Bravo V, Pippa R, Song WM, Carceles-Cordon M, Dominguez-Andres A, Fujiwara N, Woo J, Koh AP, Ertel A, Lokareddy RK, et al. (2018). Nuclear Pores Promote Lethal Prostate Cancer by Increasing POM121-Driven E2F1, MYC, and AR Nuclear Import. Cell 174, 1200–1215.e20. 10.1016/j.cell.2018.07.015. [PubMed: 30100187]
46. Vecchione L, Gambino V, Raaijmakers J, Schlicker A, Fumagalli A, Russo M, Villanueva A, Beerling E, Bartolini A, Mollevi DG, et al. (2016). A Vulnerability of a Subset of Colon Cancers with Potential Clinical Utility. Cell 165, 317–330. 10.1016/j.cell.2016.02.059. [PubMed: 27058664]
47. Borlido J, Sakuma S, Raices M, Carrette F, Tinoco R, Bradley LM, and D'Angelo MA (2018). Nuclear pore complex-mediated modulation of TCR signaling is required for naive CD4(+) T cell homeostasis. Nat. Immunol 19, 594–605. 10.1038/s41590-018-0103-5. [PubMed: 29736031]
48. Pascual-Garcia P, and Capelson M (2021). The nuclear pore complex and the genome: organizing and regulatory principles. Curr. Opin. Genet. Dev 67, 142–150. 10.1016/j.gde.2021.01.005. [PubMed: 33556822]
49. Sakuma S, and D'Angelo MA (2017). The roles of the nuclear pore complex in cellular dysfunction, aging and disease. Semin. Cell Dev. Biol 68, 72–84. 10.1016/j.semcdb.2017.05.006. [PubMed: 28506892]
50. Hampoelz B, Andres-Pons A, Kastritis P, and Beck M (2019). Structure and Assembly of the Nuclear Pore Complex. Annu. Rev. Biophys 48, 515–536. 10.1146/annurev-biophys-052118-115308. [PubMed: 30943044]
51. Lin DH, and Hoelz A (2019). The Structure of the Nuclear Pore Complex (An Update). Annu. Rev. Biochem 88, 725–783. 10.1146/annurev-biochem-062917-011901. [PubMed: 30883195]

52. Taggart JC, Zauber H, Selbach M, Li GW, and McShane E (2020). Keeping the Proportions of Protein Complex Components in Check. Cell Syst. 10, 125–132. 10.1016/j.cels.2020.01.004. [PubMed: 32105631]

53. Lam YW, Lamond AI, Mann M, and Andersen JS (2007). Analysis of nucleolar protein dynamics reveals the nuclear degradation of ribosomal proteins. Curr. Biol 17, 749–760. 10.1016/j.cub.2007.03.064. [PubMed: 17446074]

54. McShane E, Sin C, Zauber H, Wells JN, Donnelly N, Wang X, Hou J, Chen W, Storchova Z, Marsh JA, et al. (2016). Kinetic Analysis of Protein Stability Reveals Age-Dependent Degradation. Cell 167, 803–815.e21. 10.1016/j.cell.2016.09.015. [PubMed: 27720452]

55. Lau NC, Kolkman A, van Schaik FMA, Mulder KW, Pijnappel WWMP, Heck AJR, and Timmers HTM (2009). Human Ccr4-Not complexes contain variable deadenylase subunits. Biochem. J 422, 443–453. 10.1042/BJ20090500. [PubMed: 19558367]

56. Kerr SC, Azzouz N, Fuchs SM, Collart MA, Strahl BD, Corbett AH, and Laribee RN (2011). The Ccr4-Not complex interacts with the mRNA export machinery. PLoS One 6, e18302. 10.1371/journal.pone.0018302. [PubMed: 21464899]

57. Fernandez-Martinez J, and Rout MP (2009). Nuclear pore complex biogenesis. Curr. Opin. Cell Biol 21, 603–612. 10.1016/j.ceb.2009.05.001. [PubMed: 19524430]

58. D'Angelo MA, and Hetzer MW (2008). Structure, dynamics and function of nuclear pore complexes. Trends Cell Biol. 18, 456–466. 10.1016/j.tcb.2008.07.009. [PubMed: 18786826]

59. Schindelin J, Arganda-Carreras I, Frise E, Kaynig V, Longair M, Pietzsch T, Preibisch S, Rueden C, Saalfeld S, Schmid B, et al. (2012). Fiji: an open-source platform for biological-image analysis. Nat. Methods 9, 676–682. 10.1038/nmeth.2019. [PubMed: 22743772]

60. Huang T, Choi M, Tzouros M, Golling S, Pandya NJ, Banfai B, Dunkley T, and Vitek O (2020). MSstatsTMT: Statistical Detection of Differentially Abundant Proteins in Experiments with Isobaric Labeling and Multiple Mixtures. Mol. Cell. Proteomics 19, 1706–1723. 10.1074/mcp.RA120.002105. [PubMed: 32680918]

61. Szklarczyk D, Kirsch R, Koutrouli M, Nastou K, Mehryary F, Hachilif R, Gable AL, Fang T, Doncheva NT, Pyysalo S, et al. (2023). The STRING database in 2023: protein-protein association networks and functional enrichment analyses for any sequenced genome of interest. Nucleic Acids Res. 51, D638–D646. 10.1093/nar/gkac1000. [PubMed: 36370105]

Highlights

- Nucleoporin translation/degradation modulate nuclear pore complex (NPC) numbers
- The CCR4-NOT complex negatively regulates NPC formation
- Inhibition of CCR4-NOT increases nucleoporins available for NPC assembly
- Increasing NPC numbers by CCR4-NOT inhibition does not enhance nuclear import

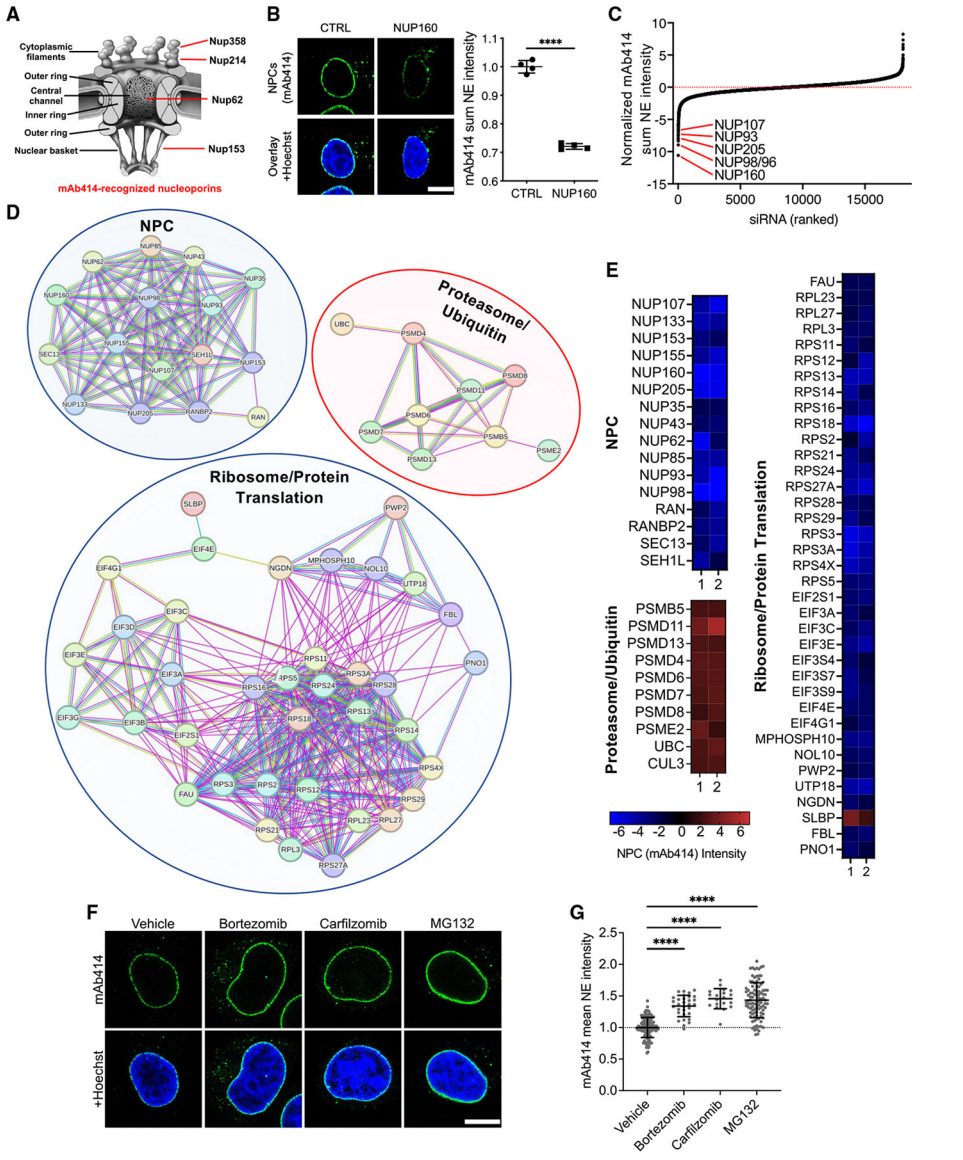

Figure 1. Whole-genome siRNA screen identifies protein translation and degradation as key modulators of NPC assembly

(A) Schematic illustration of an NPC showing the four different nucleoporins recognized by the mAb414 antibody.

(B) A375 cells treated with control or *NUP160* siRNAs for 48 h were stained with the mAb414 antibody and Hoechst before imaging by confocal microscopy. Left, images show representative nuclear cross-sections. Scale bar, 10 μm. Right, quantification of nuclear envelope (NE) mAb414 sum intensity relative to controls.

(C) Quantification of the relative change in mAb414 NE intensity after siRNA knockdown in the whole-genome siRNA screening assay. Graph shows mAb414 sum intensity normalized to controls and divided by SD of controls, representing the average number of SDs away from the control. Data show mean of two wells. Red lines highlight the relative positioning of core members of the NPC scaffold.

(D) Top nodes from STRING protein-protein interaction analysis of hits ($p \leq 0.001$) from the whole-genome siRNA screen.
(E) Heatmap of mAb414 intensity measured after siRNA knockdown of genes in clusters identified in (D); columns are technical replicates.
(F) A375 cells treated with vehicle or proteasome inhibitors for 16 h were stained with the mAb414 antibody and Hoechst before imaging by confocal microscopy. Scale bar, 10 μm.
(G) Quantification of NE mAb414 intensity measurements of cells from (F) relative to control vehicle. Data pooled from two independent experiments.
Data are represented as mean ± SD.****$p \leq 0.0001$ by two-tailed unpaired Student's t test (B) or one-way analysis of variance (ANOVA) with multiple comparisons test (G).

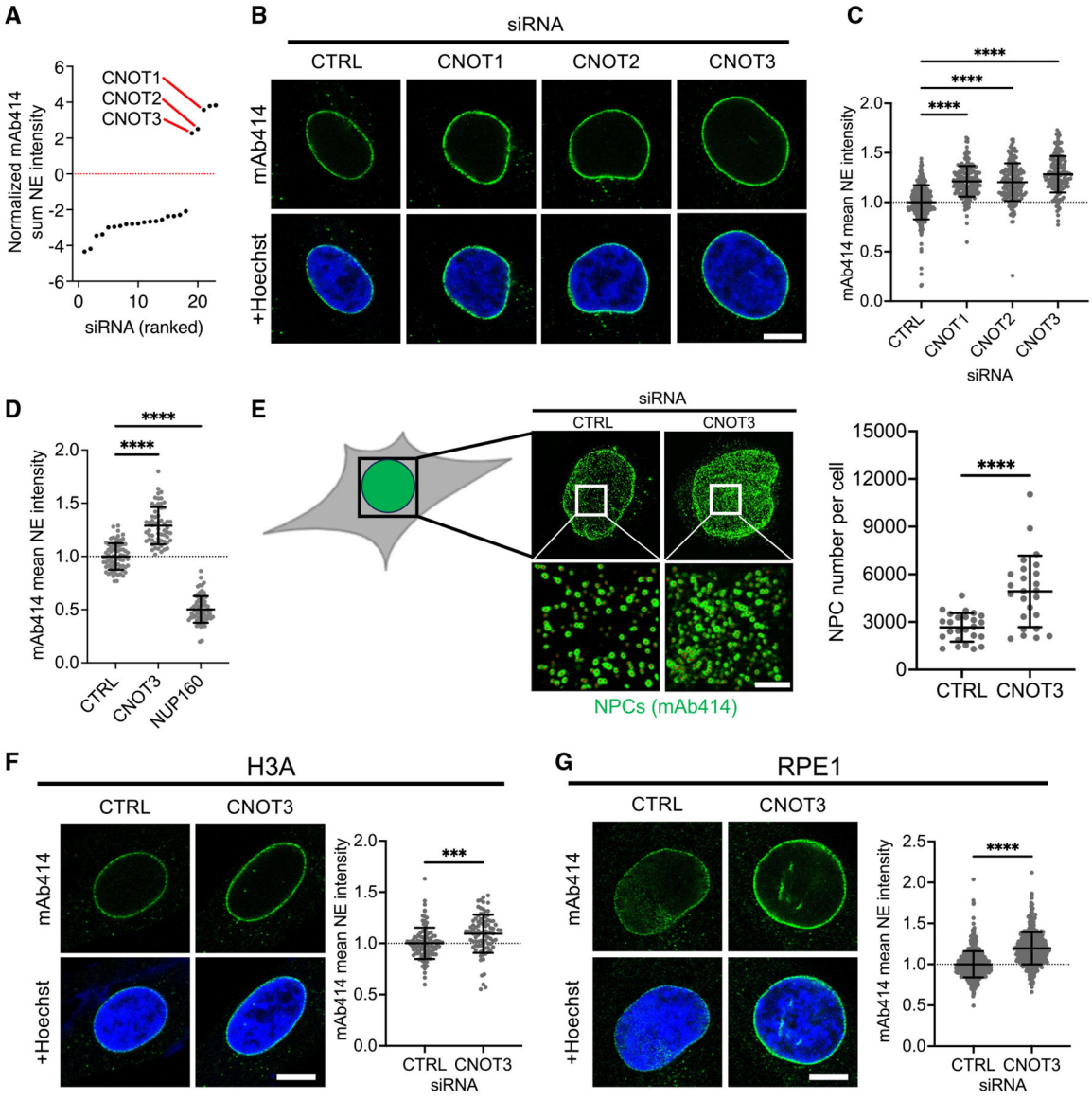

Figure 2. The CCR4-NOT complex negatively regulates NPC assembly

(A) Quantification of the relative change in mAb414 NE intensity after siRNA knockdown of genes selected from primary screen list. Graph shows mAb414 sum intensity normalized to controls and divided by SD of controls, representing the average number of SDs away from the control. Red lines highlight the relative positioning of members of the CCR4-NOT complex.

(B) Confocal imaging of A375 cells transfected with pooled siRNAs and stained for mAb414 and Hoechst. Scale bar, 10 μm.

(C) Quantification of images from (B) relative to control.

(D) Quantification of mAb414 mean NE intensity in A375 cells transfected with the indicated individual siRNAs. Quantification is normalized to control siRNA.

(E) 3D structured illumination microscopy of control and CNOT3-depleted cells stained with mAb414. Left, schematic illustration of nuclear area imaged per cell. Center,

representative images (scale bar, 10 μm); insets represent magnified areas (scale bar, 2 μm). Right, quantification of total NPC number per cell. Data pooled from two independent experiments.

(F) Confocal imaging of H3A melanocytes transfected with control or CNOT3 siRNA and stained for mAb414 and Hoechst. Left, representative images. Scale bar, 10 μm. Right, Quantification of images relative to control.

(G) Confocal imaging of RPE-1 epithelial cells transfected with control or CNOT3 siRNA and stained for mAb414 and Hoechst. Left, representative images. Scale bar, 10 μm. Right, Quantification of images relative to control. Unless specified, representative images and quantification data are from three or more independent experiments.

Data are represented as mean ± SD. ***$p \leq 0.001$; ****$p \leq 0.0001$ by one-way ANOVA with multiple comparisons test (B and C) and by two-tailed unpaired Student's t test (D–F).

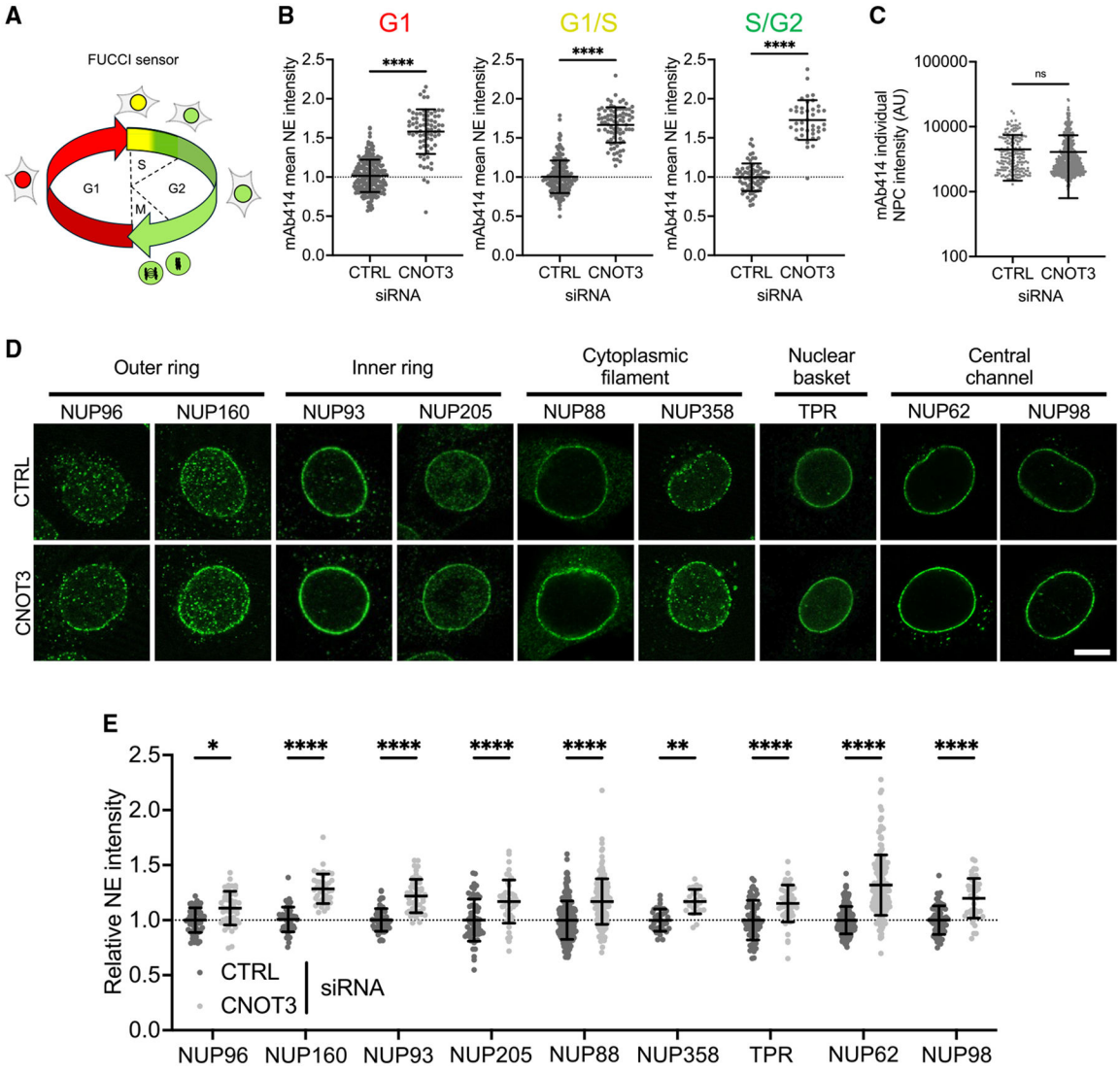

Figure 3. CNOT3 knockdown increases the number of fully formed NPCs

(A) Schematic illustration of the FUCCI cell-cycle sensor.

(B) Quantification of mAb414 mean NE intensity at different phases of the cell cycle of A375 cells expressing the FUCCI sensor and transfected with the control or CNOT3 siRNAs.

(C) Quantification of mAb414 intensity on individual NPCs identified by 3D structured illumination microscopy after transfection with control or CNOT3 siRNAs.

(D) Confocal immunofluorescence imaging of A375 cells transfected with control or CNOT3 siRNAs and stained for antibodies against selected nucleoporins. The NPC subcomplexes or NPC location for each nucleoporin are shown. Scale bar, 10 μm.

(E) Quantification of cells from (B) relative to controls. Representative images and data from two (C) or three (B, D, and E) independent experiments.

Data are represented as mean ± SD. *$p \leq 0.05$; **$p \leq 0.01$; ****$p \leq 0.0001$ by two-tailed unpaired Student's t test (B and C) or two-way ANOVA with Sidak multiple comparisons test (E).

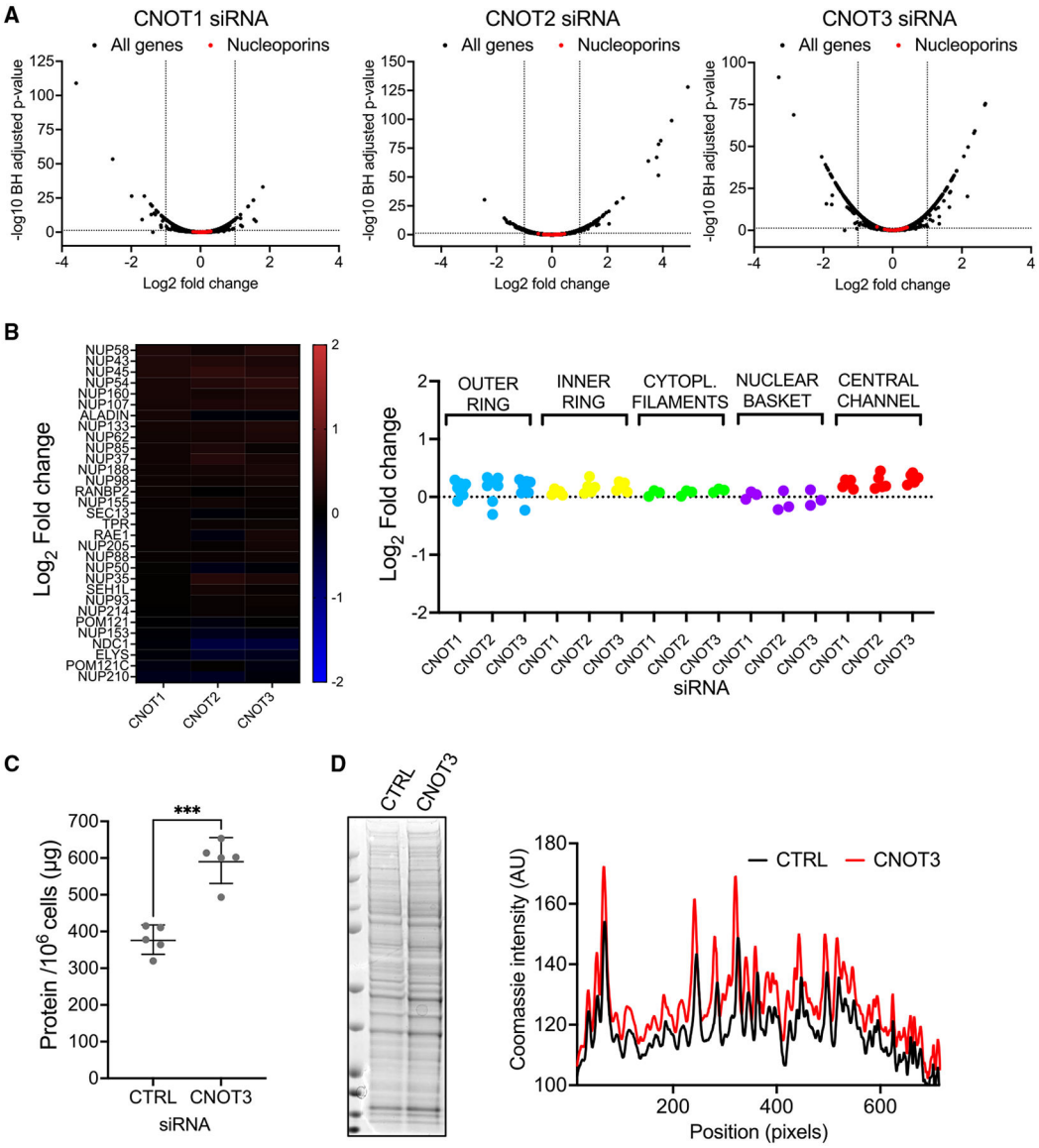

Figure 4. CNOT3 knockdown increases cellular protein levels

(A) Volcano plots of differentially expressed proteins in A375 cells transfected with CNOT1, CNOT2, or CNOT3 siRNAs relative to controls. Red dots represent nucleoporins. Vertical dotted lines indicate a 2-fold change in protein levels.

(B) Differential expression of nucleoporins by proteomics analysis after CNOT1, CNOT2, or CNOT3 siRNA relative to control siRNA treatment. Left, heatmap. Right, differential protein expression levels separated by subcomplexes of different NPC domains.

(C) Protein quantification of lysates from an equal number of cells treated with control or CNOT3 siRNAs.

(D) Coomassie blue-stained SDS-PAGE gels of lysates from equal number of control and CNOT3-depleted cells (left). Line quantification of SDS-PAGE-separated proteins (right). Representative images and quantification data are from three or more independent experiments.

Data are represented as mean ± SD. ***$p \leq 0.001$ by two-tailed unpaired Student's t test.

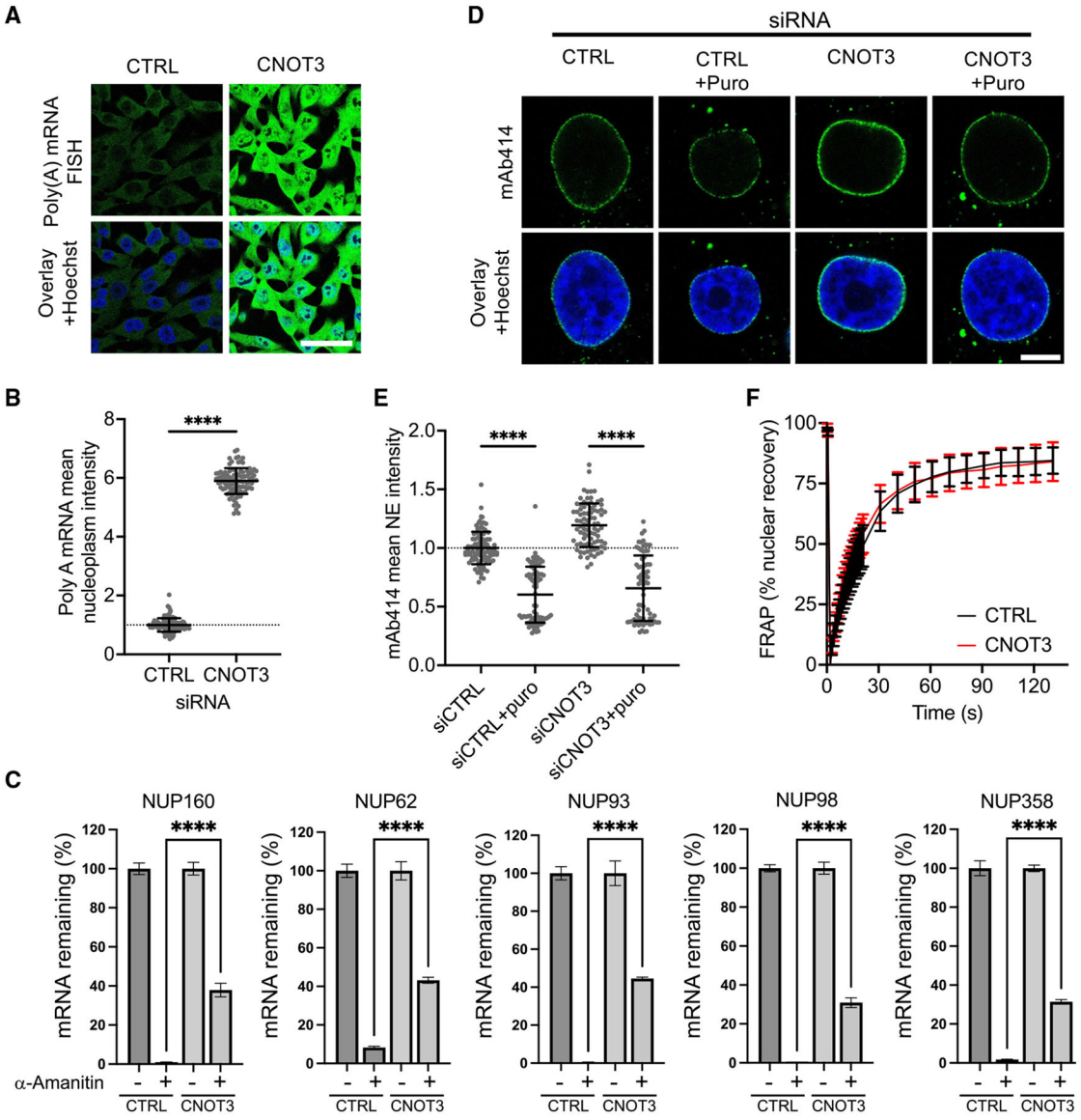

Figure 5. CNOT3 knockdown drives NPC assembly by increasing mRNA stability and protein translation

(A) Analysis of mRNA levels by poly(A) mRNA FISH of A375 cells transfected with control or CNOT3 siRNAs. Scale bar, 50 μm.

(B) Quantification of images from (A) relative to control.

(C) Percentage of nucleoporin mRNA remaining after 12 h of transcription inhibition with α-amanitin relative to untreated cells.

(D) Confocal imaging of A375 cells transfected with control or CNOT3 siRNAs for 24 h before treatment with vehicle or puromycin (Puro) for 16 h. Scale bar, 10 μm.

(E) Quantification of images from (C) relative control.

(F) Fluorescence recovery after photo bleaching (FRAP) analysis showing nuclear import of the NLS-2xGFP-NES reporter in A375 cells after treatment with control or CNOT3 siRNAs. The data are expressed as percentage of FRAP relative to pre-bleach intensity. *n* =

18 cells per condition. Representative images and quantification data are from three or more independent experiments.

Data are represented as mean ± SD. ****$p \leq 0.0001$ by one-way ANOVA with multiple comparisons test (B, C, and E) or two-tailed unpaired Student's t test (B).

KEY RESOURCES TABLE

REAGENT or RESOURCE	SOURCE	IDENTIFIER
Antibodies		
CNOT3 Mouse mAb	Abnova	Cat#: H00004849-M01A; RRID: AB_528068
mAb414 Mouse mAb	BioLegend	Cat#: 902901; RRID: AB_2564690
NUP358 (RanBP2) Rabbit pAb	Bethyl Laboratories	Cat#: A301–796A; RRID: AB_1855534
NUP98 Rabbit mAb	Cell Signaling Technology	Cat#: 13393S; RRID: AB_2728831
NUP93 Mouse mAb	Santa Cruz Biotechnology	Cat#: sc-374399; RRID: AB_10989918
NUP160 Rabbit pAb	Sigma-Aldrich	Cat#: SAB4500969; RRID: AB_10745930
NUP96 Rabbit pAb	Bethyl Laboratories	Cat#: A301–784A-T1; RRID: AB_1855530
NUP205 Mouse mAb	Santa Cruz Biotechnology	Cat#: sc-377047; RRID: AB_1129260
TPR Rabbit mAb	Santa Cruz Biotechnology	Cat#: sc-271565; RRID: AB_10649043
Beta-Tubulin Mouse mAb	Cell Signaling Technology	Cat#: 2128S; RRID: AB_823664
LAMIN B Ab Rabbit pAb	Abcam	Cat#:ab16048; RRID: AB_443298
S6 Rabbit mAb	Cell Signaling	Cat#: 2217; RRID: AB_331355
TOM70 Mouse mAb	Cell Signaling	Cat#: 98445; RRID: AB_3674095
GAPDH Goat pAb	R&D Systems	Cat#: AF5718; RRID: AB_355053
Alexa Fluor 488 Anti-Mouse IgG Polyclonal	Invitrogen	Cat#: A21202; RRID: AB_141607
Alexa Fluor 546 Anti-Mouse IgG Polyclonal	Invitrogen	Cat#: A21570; RRID: AB_2535814
Alexa Fluor 488 Anti-Rabbit IgG Polyclonal	Invitrogen	Cat#: A21206; RRID: AB_2535792
Alexa Fluor 555 Anti-Rabbit IgG Polyclonal	Invitrogen	Cat#: vA31572; RRID: AB_2536189
Chemicals, peptides, and recombinant proteins		
Bortezomib	Sigma	Cat#:5043140001
Carfilzomib	MedChemExpress	Cat#:HY-10455
MG132	Thermo Fisher Scientific	Cat#: J62350
Puromycin	Gibco	Cat#:A1113803
α-Amanitin	Cayman Chemical	Cat#:17898
Critical commercial assays		
PureLink RNA Mini kit	Thermo Fisher Scientific	Cat#:12183018A
QuantiTect Reverse Transcription Kit	Qiagen	Cat#: 205313
Lipofectamine™ RNAiMAX Transfection Reagent	Invitrogen	Cat#:13778075
TaqMan Fast Advanced Master Mix	Applied Biosystems	Cat#: 4444554
Deposited data		
Raw Proteomics Data	This paper	ProteomeXchange PXD052767
Experimental models and study participant details: Cell lines		
Human: A375	ATCC	CRL-1619
Human: RPE1	Laboratory of Andrew Holland	N/A
Human: Hermes 3A (H3A)	Laboratory of Ze’ev Ronai	N/A

REAGENT or RESOURCE	SOURCE	IDENTIFIER
Oligonucleotides		
All siRNAs information are found in Table S3	This paper	N/A
GAPDH forward primer 5′-GACAGTCAGCCGCATCTTCT-3′	Integrated DNA Technologies	N/A
GAPDH reverse primer: 5′-ACCAAATCCGTTGACTCCGA_3′	Integrated DNA Technologies	N/A
CNOT3 forward primer: 5′-ACGAGTTTGAGCAGGGCA-3′	Integrated DNA Technologies	N/A
CNOT3 reverse primer: 5′-GGTAGCGGTACTCAAAGGTGA-3′	Integrated DNA Technologies	N/A
NUP62 Taqman primers		Hs02621445_S1
NUP93 Taqman primers		Hs00206418_m1
NUP98 Taqman primers		Hs00180522_m1
NUP160 Taqman primers		Hs00299567_m1
NUP358 (RANBP2) Taqman primers		Hs01108571_m1
GAPDH Taqman primers		Hs03929097_g1
HPRT1 Taqman primers		Hs028000695_m1
SRSF3 Taqman primers		Hs01122144_m1
Recombinant DNA		
pTripz Control shRNA lentivirus vector	Dharmacon	RHS4743
pTripz NUP160 shRNA lentivirus vector	Dharmacon	V2THS_101965
pTripz CNOT3 shRNA lentivirus vector	Dharmacon	V2THS_87050
pLV NLS-2xGFP-NES lentivirus vector	VectorBuilder	This study
pT7-EGFP-C1-HsNot3	Addgene	37372
Software and algorithms		
ImageJ (Fiji)	Schindelin et al.[59]	https://imagej.net/Fiji
ImageJ Macro code for cell region identification and quantification in Data S1	This paper	N/A
FlowJo	BD Life Sciences	https://www.flowjo.com/
MSstatsTMT R package	Huang et al.[60]	https://msstats.org/msstatstmt/
Harmony HCS software	PerkinElmer	N/A
Genedata Screener software	GeneData	N/A
STRING database (version 12)	Szklarczyk et al.[61]	https://string-db.org/